Optical Engineering

OpticalEngineering.SPIEDigitalLibrary.org

Review of GaN-based devices for terahertz operation

Kiarash Ahi

SPIE.

Kiarash Ahi, "Review of GaN-based devices for terahertz operation," *Opt. Eng*. **56**(9), 090901 (2017), doi: 10.1117/1.OE.56.9.090901.

Optical Engineering 56(9), 090901 (September 2017)

REVIEW

Review of GaN-based devices for terahertz operation

Kiarash Ahi*
University of Connecticut, Storrs, Connecticut, United States

Abstract. GaN provides the highest electron saturation velocity, breakdown voltage, operation temperature, and thus the highest combined frequency-power performance among commonly used semiconductors. The industrial need for compact, economical, high-resolution, and high-power terahertz (THz) imaging and spectroscopy systems are promoting the utilization of GaN for implementing the next generation of THz systems. As it is reviewed, the mentioned characteristics of GaN together with its capabilities of providing high two-dimensional election densities and large longitudinal optical phonon of ~90 meV make it one of the most promising semiconductor materials for the future of the THz emitters, detectors, mixers, and frequency multiplicators. GaN-based devices have shown capabilities of operation in the upper THz frequency band of 5 to 12 THz with relatively high photon densities in room temperature. As a result, THz imaging and spectroscopy systems with high resolution and deep depth of penetration can be realized through utilizing GaN-based devices. A comprehensive review of the history and the state of the art of GaN-based electronic devices, including plasma heterostructure field-effect transistors, negative differential resistances, hetero-dimensional Schottky diodes, impact avalanche transit times, quantum-cascade lasers, high electron mobility transistors, Gunn diodes, and tera field-effect transistors together with their impact on the future of THz imaging and spectroscopy systems is provided. *© 2017 Society of Photo-Optical Instrumentation Engineers (SPIE)* [DOI: 10.1117/1.OE.56.9.090901]

Keywords: GaN; terahertz; millimeter wave; imaging; spectroscopy; characterization; heterostructure field-effect transistors; negative differential resistance; hetero-dimensional Schottky diodes; impact avalanche transit time; quantum-cascade lasers; high electron mobility transistor; Gunn diodes, tera field-effect transistor.

Paper 170903VP received Jun. 13, 2017; accepted for publication Aug. 16, 2017; published online Sep. 11, 2017.

1 Introduction

Among commonly used wide bandgap semiconductor materials, GaN provides the highest bandgap energy, electron saturation velocity, and thermal conductivity. GaN has been a well-known semiconductor material for electroluminescent visible light diodes since their first introduction in 1971.[1,2] The urge for renewable energy systems and electric cars has promoted the application of GaN in power electronic converters.[3] GaN-based devices provide high switching frequency and high power,[4] which are needed for realization of the next generation of the electric grid, namely, the smart grid,[5] and electric vehicles.[6] High-frequency converters need less passive storage elements and are attractive for vehicle applications in terms of size, weight, reliability, and cost.[7] Among the emerging systems in photonics, with developing the first terahertz (THz) imaging system in no more than two decades ago,[8] THz systems including THz-time-domain spectroscopy (TDS) and THz-continuous wave (CW) imaging systems are developed with a fast pace. Thanks to low photon energy in the THz regime, the THz beam can traverse through most of the nonmetallic materials. x-ray photons can also traverse through nonmetallic materials. However, high-energy x-ray photons ionize the molecules of the object. Ionization is harmful to wide varieties of objects as it causes cancer for live tissues[9] and degrades semiconductor devices.[10] For avoiding degrading effects, for investigation of valuable historical artifacts,[11] x-ray and chemicals might not be recommended. In addition, detaching the historical structures, such as wall paintings, to place them in a protected x-ray imaging chamber is not feasible. Although the degrading effect of intense THz radiation on DNA is reported,[12–14] no other degrading effect is observed, and THz is still considered to be safer than x-ray in many areas. As a result, THz spectroscopy and imaging systems provide promising substitutes for ionizing x-ray and invasive chemical characterization tools in wide varieties of applications.[15] THz-TDS systems are powerful tools for material spectroscopy, layer inspection, and transmission imaging of packaged objects.[16] These capabilities of THz-TDS systems are utilized in authentication,[17–19] nondestructive inspection of composite materials,[20–28] three-dimensional imaging,[29–32] metrology and quality control of industrial products,[33–37] detection of concealed weapons,[38–45] art investigations,[46,47] tomography,[48–52] biomedical diagnosis,[53–56] material characterization,[57–62] thickness measurement,[63,64] and holography.[65–68]

Despite this variety of applications, THz systems are suffering from two major drawbacks, namely, (1) low resolution and (2) low photon intensity. Low resolution is the intrinsic feature of THz systems. According to the Gaussian beam and diffraction theories, the focused beam diameter, divergence, and bending of the beam are directly related to the wavelength.[69] Common THz imaging systems are not capable of generating THz beams of higher than 5 THz. Moreover, the attenuation of the beam drops exponentially with respect to the wavelength, transmission imaging with beams with frequencies of higher than 1.5 THz has not been possible yet. This deficiency is shown in Fig. 1. As this figure indicates, the signal-to-noise ratio (SNR) of the generated beam via conventional GaAs-based photoconductive antennas (PCA) drops to zero by 4 THz and the intensity of the beam after passing through the sample, which in this case

*Address all correspondence to: Kiarash Ahi, E-mail: kiarash.ahi@uconn.edu

0091-3286/2017/$25.00 © 2017 SPIE

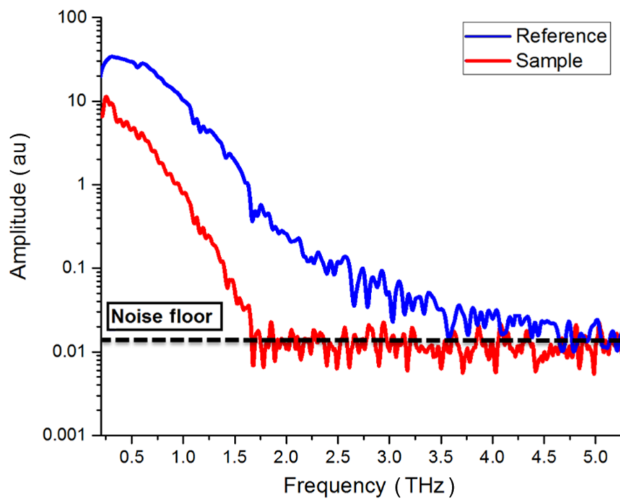

Fig. 1 The SNR of the generated beam by conventional GaAs-based PCA drops to zero by 4 THz. When a 2.3 packaged IC is placed as the sample in the system, the SNR drops to zero at frequencies below 2 THz.

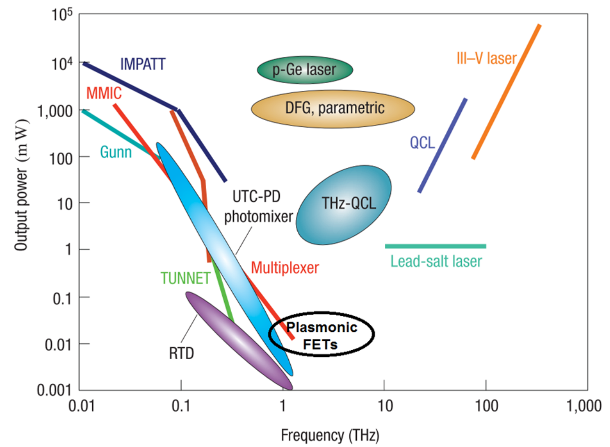

Fig. 3 Superiority of GaN-based devices over other devices in THz regime. Updated and reprinted from Ref. 92, with permission of Nature Publishing Group.

was a 2.3-mm packaged integrated circuits (IC), drops to zero for frequencies above 2 THz.[70]

A great deal of research is dedicated to the enhancement of the resolution of the THz imaging systems. In this regard, different groups are working on the enhancement of the resolution by approaching it from different aspects. Stantchev et al.[71] have proposed a near-field THz imaging of hidden objects using a single-pixel detector. However, the drawback of near-field imaging is the fact that objects thicker than a few hundred micrometers cannot be imaged. Trofimov et al.[72,73] have realized conventional image processing techniques for increasing the quality of THz imaging systems. Kulya et al.[74] have proposed taking material dispersion into account for enhancing the quality of THz images. For suppressing the absorption in the physical lenses, diffraction lenses with low absorptions are proposed.[75–78] Ahi and Anwar,[79] Ahi et al.[80] have proposed a mathematical algorithm to incorporate the THz imaging features into Gaussian beam theory in order to model the THz point spread function and demerge the merged feature through deconvolution. Chernomyrdin et al.[81] have achieved promising resolution enhancement by utilizing solid immersion imaging and wide-aperture spherical lens.[82] In another trend, for the enhancement of the imaging systems, subwavelength focusing using hyperbolic meta materials is proposed by Kannegulla et al.[83–85] However, as it will be discussed in this paper, GaN-based devices can fundamentally address the resolution by enabling THz imaging systems with frequencies higher than 5 THz and enhancing the photon intensity. For instance, GaN-based quantum-cascade lasers (QCL) can operate in 5 to 12 THz,[86] whereas the operation of conventional naturally cooled GaAs-based QCLs in the upper THz frequency band is limited by longitudinal-optical (LO) phonon of 36 meV.[87]

For overcoming the large beam diameter, diffraction, and absorption issue, THz imaging and spectroscopy systems that can operate in the upper THz frequency band and with higher photon densities are needed. Wide bandgap semiconductor devices provide promising features for implementing such devices. Figure 2 shows the numerical values of characteristics of GaN and GaAs. The bandgap energy, saturation velocity, and thermal conductivity of GaN are all more than twice of those of GaAs. As a result, GaN devices offer higher output power and operation frequency compared with other conventional III to V devices.[88–91] The mentioned characteristics of GaN together with its capabilities of providing high two-dimensional (2-D) election densities and high LO phonon of ∼90 meV make it one of the most promising semiconductors for the future of the generation, detection, mixing, and frequency multiplication of the electromagnetic waves in THz frequency regime. As Fig. 3 shows, plasmonic GaN-based heterostructure field-effect transistors (HFETs) and QCL have capabilities of operating in the upper THz frequency band of 5 to 12 THz, in room temperature and with relatively high emission powers.[92–94]

In this paper, a comprehensive review of the history and state-of-the-art of the GaN-based electronic devices and their impact on the future of THz imaging and spectroscopy systems is provided. Plasma HFETs, negative differential resistances (NDRs), hetero-dimensional Schottky diodes (HDSDs), impact avalanche transit times (IMPATTs), QCLs, high electron mobility transistors (HEMTs), Gunn diodes, and tera field-effect transistors (TeraFETs) together with their impact on the future of THz imaging and spectroscopy systems are reviewed. Challenges that are in front of scientific groups for implementing GaN devices are discussed, and a detailed report on the timeline and state of the art of achievements

	Bandgap energy (Eg)	**critical field (E_{CR})**	**Saturation velocity (V_{SAT})**	**thermal conductivity**
GaN ✓	**3.4 (eV)**	**2 (MV/cm)**	**2×107 (cm/sec)**	**1.3 (W/cm)**
GaAs	**1.4 (eV)**	**0.4 (MV/cm)**	**1×107 (cm/sec)**	**0.5 (W/cm)**

Fig. 2 Comparison between GaN and GaAs.

of different research groups in developing models, theories, and implementing practical GaN THz devices is given. Characterization techniques of GaN in THz frequency range are reviewed as well.

This paper is organized as follows: Sec. 2 provides a review of the history and state-of-the-art of GaN for THz applications. Section 3 reviews characterization techniques of GaN in the THz frequency range. Section 4 concludes this paper and proposes a roadmap for utilization of GaN in order to address the growing demands of THz imaging and spectroscopy systems.

2 GaN–Based THz Devices

In this section, a brief history of GaN-based devices for THz applications is reviewed. Then, GaN-based electronic devices for generation, detection, mixing, and frequency multiplication of the electromagnetic waves in THz frequency regime are reviewed. GaN-based plasma THz heterostructure field effect transistors (HFETs), NDR diode oscillators, HDSDs, impact avalanche transit time diodes, planar Gunn diode, antenna-coupled field-effect transistors, and quantum cascade lasers are discussed.

2.1 *Importance of GaN in Plasma HFETs*

III-N two-dimensional electron gas (2DEG) has exceptional transport characteristics. As a result, GaN-based devices have been proposed as promising advanced plasmonic electronic devices for detection, mixing, and generation of THz radiation.[95] Particularly, GaN provides exceptional characteristics for implementation of plasma HFETs. The fundamental plasma frequency is given by

$$\omega_0 = \frac{\pi s}{2L}, \tag{1}$$

where L is the length of the channel and s is the speed of propagation. In a FET, eigenmodes of the plasma oscillations are odd harmonics of the fundamental plasma frequency. Hence, in order to enable HFET to operate in plasma mode, the length of the channel needs to be limited to the following condition:

$$L \ll L_{\mathrm{cr}} = \frac{s\mu m}{r}. \tag{2}$$

where p is mobility in low field and m is the effective mass of the electron. This condition is satisfied when

$$\omega_0 \tau \gg 1, \tag{3}$$

where τ is the momentum relaxation time. Consequently, the frequency of operation ω_{cr} needs to be much higher for HFET to work in plasma mode

$$\omega_{\mathrm{cr}} = 1/\tau. \tag{4}$$

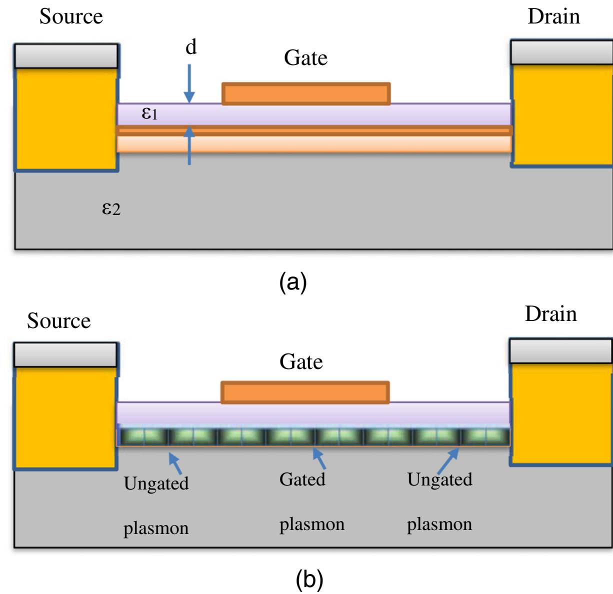

Fig. 5 An FET operating in (a) a conventional regime and (b) a plasmonic regime using the propagation of the wave of the electron density (plasma waves). Redrawn from Ref. 93.

As it is indicated in Fig. 4, ω_{cr} happens to be in the THz regime for GaN for the entire temperature of operation range.[96] An FET operating in a conventional regime and in a plasmonic regime using the propagation of the wave of the electron density is shown in Fig. 5.

2.2 *History of GaN-Based Devices for THz Applications*

With the first reported direct determination of a laser frequency in the far infrared[97] and optical frequency shifting of a mode-locked laser beam[98] both in 1967, generation and detection of electromagnetic radiation in THz frequency range are not older than 5 decades. The utilization of GaN for THz application is even younger with the first proposed AIGaN/GaN HFET for detection of THz radiation in 1997.[99] Figure 6 shows the first proposed measurement set-up of this GaN HFET in 1997. Karl-Suss Microwave Probe Station was used as the platform of the device. Two GGB microwave probes are used in the setup. The microwave power is fed to the GaN-HFET through one of the GGB microwave probes while another GGB microwave probe connects the drain of the device to the broadband bias tee. Figure 6 shows the detector responsivity for the proposed GaN HFET with the gate length $L = 5$ pm, the gate bias $U_G = -1$ V, and the threshold voltage $U_T = -2$ V. Achieving responsivity up to 0.02 THz using GaN-HFET in nonresonance mode lead to the first predictions that operating frequencies of these devices could be pushed into the THz range of frequencies in order to use

Material	Si (300 K)	Si (77 K)	GaAs (300 K)	GaAs (77 K)	GaN (300 K)	GaN (77 K)
ω_{cr} (THz)	1.7	0.46 ✗	3.5	0.093 ✗	10 ✓	1.6 ✓

Fig. 4 Material critical frequencies of operation.

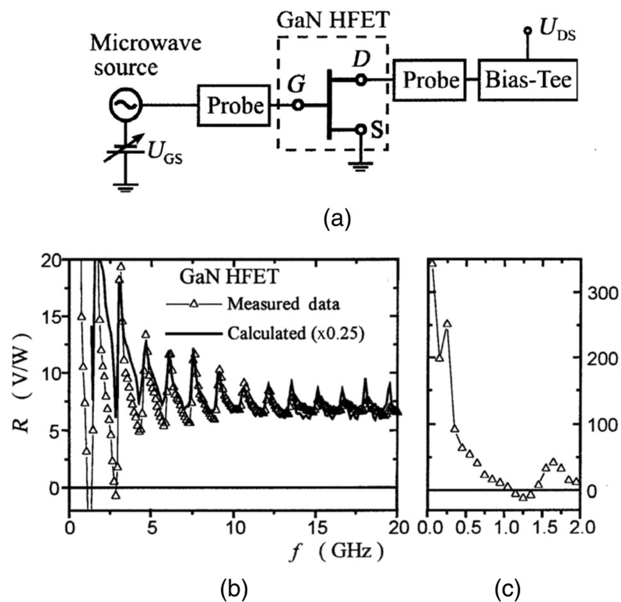

Fig. 6 (a) The measurement set-up of the detector using a GaN HFET. (b) Measured frequency dependence of the detector responsivity for a GaN HFET with the gate length $L = 5\ \mu$m, the gate bias $U_G = -1$ V, and the threshold voltage $U_T = -2$ V. The solid line shows the predicted dependence with $C = 1.2$ to 10^{-7} F/m, $(U_{GS} - U_T) = 1$ V, $\mu = 0.1\ m^2/V\,s$. (c) The full data of (c) at frequencies between 0.05 and 2 GHz. Reprinted from Ref. 99, with permission of IEEE.

them as detectors, mixers, and sources. The photoresponse of these devices in nonresonance mode was improved to 10 mv for up to 0.6 THz in room temperature by 2002.[100]

2.3 *Implementation of Resonance-Mode HFETs for Detection of THz Radiation*

The responsivities of the mentioned HFET in Sec. 2.2 exceed that of the Schottky diodes, which have been conventionally used as detectors and mixers in the THz regime.[101] The HFET detectors work at two modes of frequencies. At the low-frequency mode, the HFET works in a nonresonant mode. The responsivity in this mode can be up to 600 V/W. The frequency in this mode of operation for the fabricated HFET is 0.05 to 20 GHz as Fig. 6 shows. At the high-frequency mode, which is typically much higher than the cutoff frequency, the HFET operates in a resonance mode. The resonance happens at the plasma oscillation frequency. This is due to the fact that when the electron density in the channel of HFET is high, instead of holding the 2DEG condition, 2-D electron fluid model holds. In a 2-D electron fluid, hydrodynamic equations analogous to water in a shallow channel are applicable. Plasma waves would appear in a similar manner that waves in the water appear. The velocity of the plasma waves depends on the gate bias and is higher than the electron saturation drift velocity. As a result, a new generation of devices with frequencies higher than the radio and microwaves could be realized. The peak responsivity in this mode is higher than that of the standard Schottky diode detector. The resonance peak appears at several THz in deep submicron devices. As a result, such AlGaN/GaN HFETs can work at frequencies much higher than the cutoff frequency and thus is a proper choice for THz applications. The mentioned phenomenon does not hold in GaAs HEMTs. As a result,

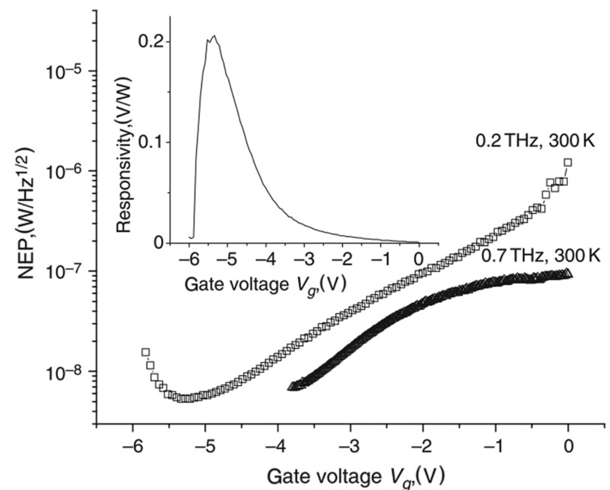

Fig. 7 NEP against gate voltage ($T = 300$ K) inset: responsivity against gate voltage for $f = 0.2$ THz.[105]

GaAs HEMTs work at frequencies much lower than cutoff frequency[99,102] and were not proposed for THz applications. However, it needs to be mentioned that the original observations of infrared absorption[103] and emission[104] related to plasma waves in silicon inversion layers date back to 1977 and 1980, respectively. Although the operation of GaN-HFETs in resonance mode for THz applications was predicted in 1997, it was practically realized in 2006 with a maximum responsivity of 0.2 V/W for 0.2 THz at room temperature.[105] Figure 7 shows the noise equivalent power (NEP) and responsivity against gate voltage of this device.

2.4 *GaN-Based Quantum Cascade Lasers*

In the conventional semiconductor lasers, a photon is emitted as the result of the recombination of a conduction band electron with a valence band hole. The frequency of the emitted photon is equal to the energy difference between the conduction band and the valence band E_g divided by the Planck constant h. The photon energy in the THz range is less than the energy gap between the conduction and valence bands of the active materials and thus for emitting THz photons, energy gaps with lower energies are needed. Intersubbands (ISBs) are introduced by realizing quantum wells (QWs). Through growing several repeated periods of QWs, usually by molecular beam epitaxy (MBE), THz-QCLs have been implemented. Not long after the first implementation in 1994 by a group of scientists including Alfred Y. Cho, known as the father of MBE, QCL became one of the most widely used approaches for generation of THz radiation.[106] The first THz-QCL was reported in 2002. It was realized by GaAs/AlGaAs heterostructures. It could emit high output powers of more than 2 mW at 4.4 THz. However, it could only operate at temperatures up to 50 K in pulsed mode.[107] The mentioned QCL could not operate in CW mode. By 2005, GaAs/AlGaAs-based QCLs have been improved to operate at 164 and 117 K in pulsed mode and CW, respectively.[108] However, operation of GaAs-based QCLs are limited by LO phonon of 36 meV. LO phonon for GaN is located at 92 meV.[87] According to the studies by the research group of Paiella and Moustakas at Boston University, as shown in Fig. 8, the population inversion and hence the gain coefficient of the GaN/AlGaN QWs dependence on

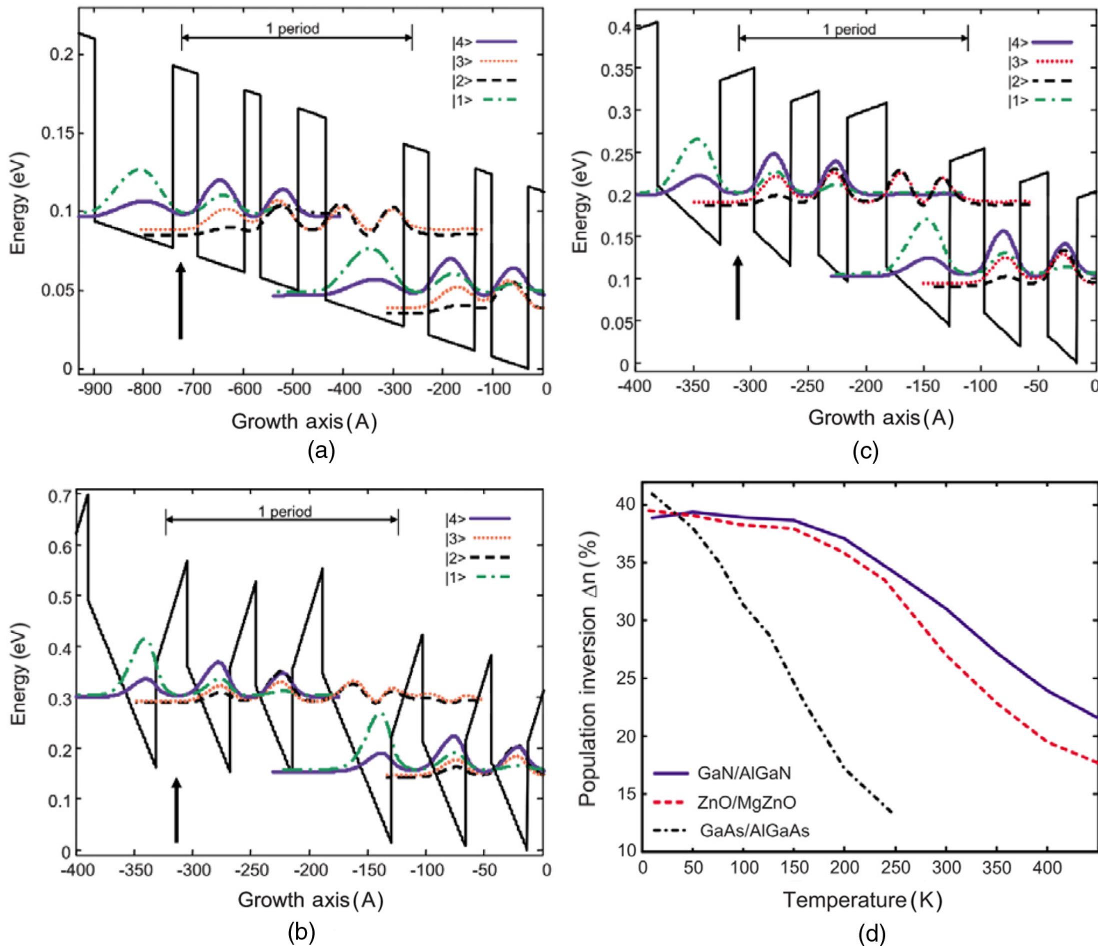

Fig. 8 Conduction-band profile and squared envelope functions of (a) the $GaAs/Al_{0.15}Ga_{0.85}As$, (b) the $GaN/A_{l0.15}Ga_{0.85}N$, and (c) the $ZnO/Mg_{0.15}Zn_{0.85}O$ QC gain media considered in this study. (d) Calculated fractional population inversion of the THz-QC structures of (a) (dash-dotted line), (b) (solid line), and (c) (dashed line), as a function of temperature. Reprinted from Ref. 109, with permission of AIP.

the temperature is three times smaller than that of GaAs/AlGaAs for THz emission and the gain coefficient of the nitride device remain large enough for laser action even without cryogenic cooling.[109–111] As a result, GaN-based devices can operate in the upper THz frequency of 5 to 10 THz at room temperature, which is inaccessible by GaAs-based devices.[86] In 2003, pioneer works reported THz emission from InGaN/GaN multiple QWs.[112,113] In the latest approach in 2015, THz-QCLs have been fabricated via radio-frequency MBE (RF-MBE) and a metal-organic chemical vapor deposition (MOCVD) on MOCVD-growth AlGaN/AlN templates grown on c-plane sapphire substrates. The number of active regions and wave-functions, contributed to lasing, were limited to be two QWs and three subband levels, respectively. As a result, lasing at ∼5.5 and ∼7.0 THz is achieved, which were the highest reported emissions for THz-QCLs up to date.[86,114,115] In the latter work, the selective injection into the upper lasing level and a wide dynamic range of operating current density are realized in order to achieve a higher operating temperature of the THz-QCL. Toward this aim, indirect injection scheme as shown in Fig. 9(a) is considered as the dynamic range of operating current density is not limited by subband alignment of narrow E_{32}. As Fig. 9(b) shows, the highest reported operation temperature for GaAs/AlGaAs is 160 K for a 1.9-THz-QCL and 150 K for a 3.8-THz-QCL, whereas GaN-based QCLs can work at room temperature.[116–118] The schematic of the overall GaN-based THz-QCL device is shown in Fig. 9(c).

AlGaN/GaN QWs are also proposed for absorption of THz radiation.[119] Reduction in Al mole fraction causes the QW width to increase, and thus ISB transitions in these QWs are adjustable to be between 1.0 to 10 μm.[120] For absorption in the THz frequency range, plasma-assisted MBE with tunable absorption from 53 to 160 μm, with respect to doping level and geometrical variations, has been reported.[121] In 2016, researchers from Boston University reported photocurrent peaks near 10 THz for THz-ISB photodetectors, which are developed based on GaN/AlGaN QWs grown on a free-standing semipolar GaN substrate.[122] Photocurrent spectrum and the conduction-band lineup of the semipolar GaN/AlGaN QW infrared photodetector (QWIP) developed by this research group, as shown in Fig. 10.

2.5 *GaN-Based Negative Differential Resistance Diode Oscillators*

Diodes with NDR have been conventionally used for generation of high-frequency high-power microwave signals. In this regard, GaAs and InP Gunn diodes can be named.

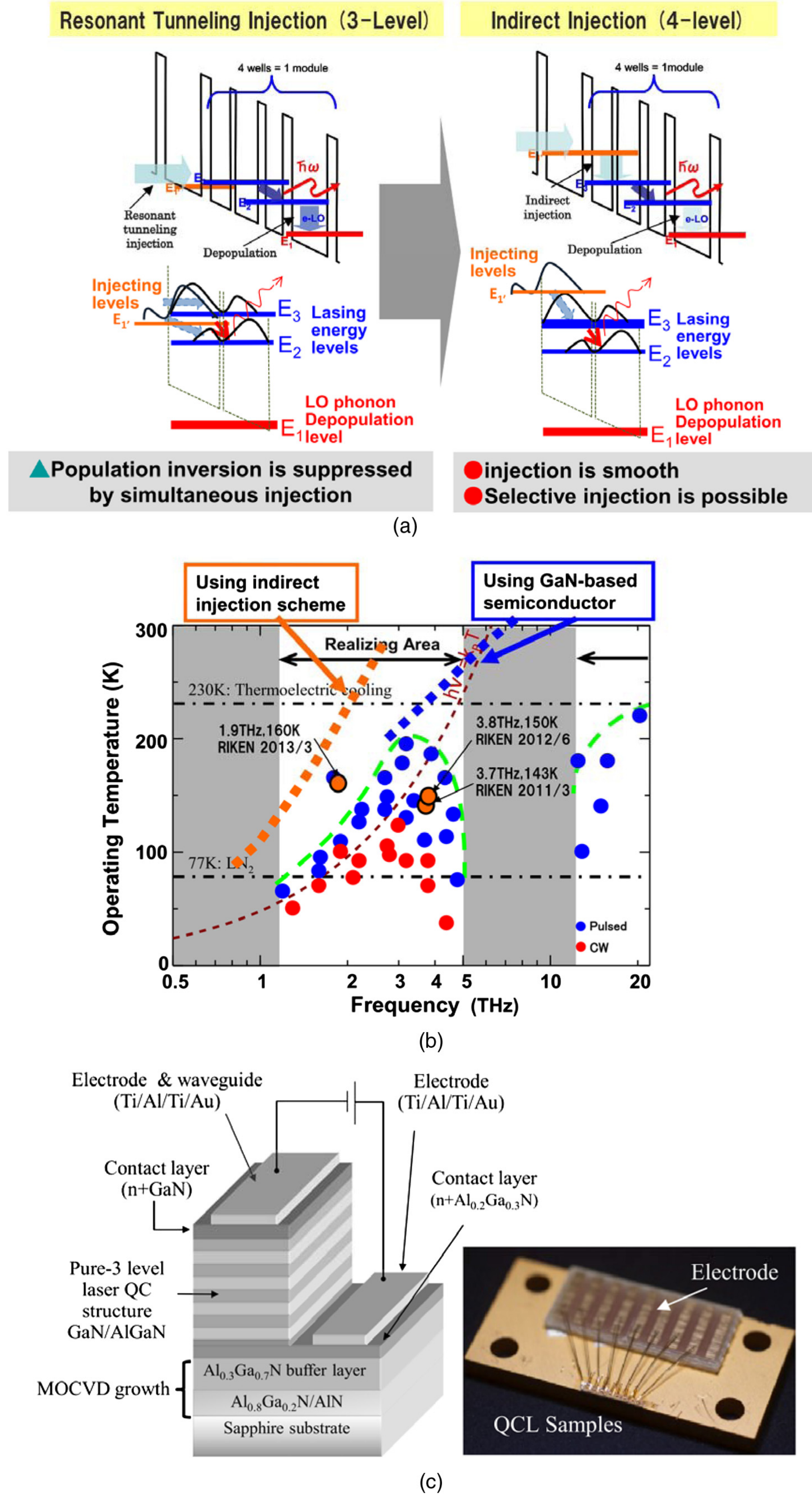

Fig. 9 (a) Schematic view of QC structures for resonant tunneling injection scheme (three-level) and indirect injection scheme (four-level). (b) Superiority of GaN-based QCLs in THz regime. (c) Schematic of the overall GaN-based THz-QCL device structure and the device photograph after having mounted to the heat sink. Reprinted from Refs. 86 and 94, with permission of SPIE.

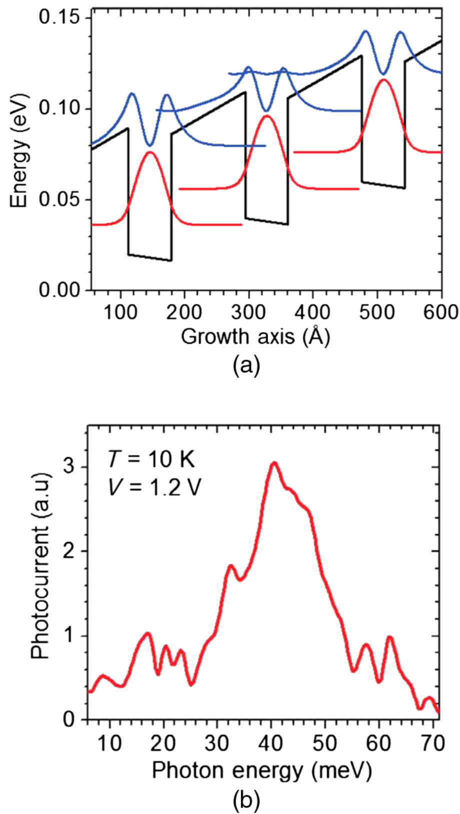

Fig. 10 (a) Conduction-band lineup of the semipolar GaN/AlGaN QWIP developed in this work, under an externally applied voltage bias of about 20 mV/period. The squared envelope functions of the bound-state subbands of each well are also shown, referenced to their respective energy levels. (b) Photocurrent spectrum measured at 10 K under an applied voltage of 1.2 V. Reprinted from Ref. 122, with permission of AIP.

Energy-relaxation time in GaAs is around 10 ps. As a result, GaAs exhibits sharp suppression in output power in frequencies higher than 100 GHz and thus cannot be used for the upper THz band applications. Wide-bandgap III to V nitrides exhibit bulk NDR effect in threshold fields above 80 kV/cm.[123] In addition, thanks to shorter energy relaxation time in GaN among other conventional III to V semiconductor materials,[124] GaN-based NDR diode oscillators offer much higher electron velocity and reduced time constants compared to conventional GaAs Gunn diodes. As a result, GaN-based NDR diodes can generate frequencies in the THz regime. The NDR relaxation frequency f_{NDR} of GaAs is reported as ∼100 GHz, whereas it is ∼1 THz for GaN-based NDR devices for intervalley transfer-based NDR, and ∼4 THz for of inflection-based NDR. The first GaN-NDR was fabricated through growing GaN layer using metalorganic vapor-phase epitaxy (MOVPE) by a research group at the University of Michigan in 2000.[125,126] The schematic and output power spectrum of THz GaN-based NDR oscillator is shown in Fig. 11. In this device, a 3-μm thick, n-type with a doping concentration of 1×10^{17} cm^{-3} GaN active layer is sandwiched between anode and cathode, which are both made of GaN with thicknesses and doping concentrations of 0.1 μm and 1×10^{19} cm^{-3}, respectively. The diameter of the diode is 50 μm. GaN active layer can be doped significantly higher than that of GaAs. As a result, current levels, and thus output

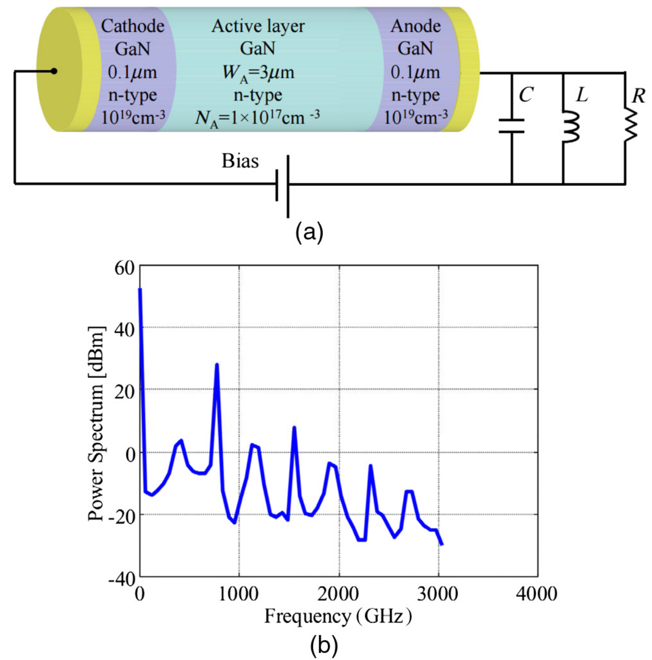

Fig. 11 (a) Schematic of GaN NDR diode oscillator. (b) Simulated output power spectrum of THz-GaN-based NDR oscillator.[126]

powers, of GaN devices can be up to four times higher than that of GaAs-based devices.

2.6 *GaN Hetero-Dimensional Schottky Diode for THz Detection*

The first experimental demonstration of THz detection by AlGaN/GaNHDSD for detection of THz radiation has been realized in 2006 by researchers from Rensselaer Polytechnic Institute.[127] The schematic of this device is shown in Fig. 12. AlGaN/GaN HDSD exhibited reasonable performance in 2.24 THz and higher frequencies. Compared with AlGaAs/InGaAs/GaAs-based THz detectors that were first reported in 1992 by the same research group,[128] the cutoff frequency of AlGaN/GaN-based HDSD device is tremendously higher. This superiority of AlGaN/GaN-based HDSD has been achieved thanks to the high 2DEG concentration, which is up to 20 times higher than that of the GaAs-based devices. This high 2DEG concentration lowers the series resistance tremendously.

2.7 *GaN-Based Impact Avalanche Transit Time Diodes for THz Frequency Range*

Monte Carlo simulations of GaN-based IMPATT diodes predict a promising role for these devices in the THz frequency range. The maximum is predicted to occur at 0.45 THz, and the cutoff frequency is on the order of 0.7 THz. The high-frequency operation of GaN-based IMPATT diodes is achievable thanks to superiorities of GaN over GaAs and Si. These superiorities can be named as, high electron drift velocity, high ionization rates, and less pronounced electron relaxation. In addition, thanks to high thermal conductivity of GaN, these devices can operate at high DC current densities.[129] Moreover, in such devices, fluctuations of the space charges affect the generation of electron–hole pairs as a negative feedback. As a result, the avalanche noise is

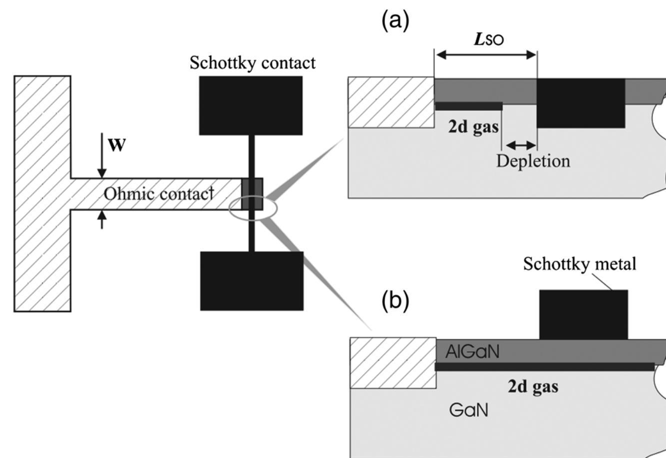

Fig. 12 Schematic of (a) lateral and (b) vertical Schottky diode under study. Reprinted from Ref. 127, with permission of IEEE.

predicted to be suppressed up to three times of magnitude for the current multiplication factor greater than ten.[130]

2.8 *GaN-Based Planar Gunn Diode for Terahertz Applications*

In 2016, researchers from Xidian University proposed a GaN-based planar Gunn diode for THz applications. Utilizing GaN provides high electron concentration of 2DEG which helps the fast formation of the dipole domain layer. Hence, the dead zone length is decreased by reducing the recess layer near the cathode which results in enhancing the RF output power.[131] For reducing the dead zone, donor-like traps near the cathode are removed. As a result, the electron concentration of this region becomes higher than other regions, and thus it acts as a n^+ doped layer of the Gunn diode. The schematic structure of GaN-HEMT liked planar Gunn is shown in Fig. 13.

2.9 *GaN-Based High-Electron-Mobility Transistors as Terahertz Detectors Based on Self-Mixing*

As pioneers, Sun et al.[132] fabricated a GaN/AlGaN HEMT using optical lithography in 2011. This GaN/AlGaN HEMT can work at room temperature and detect THz radiation via self-mixing with a responsivity of 3.6 kV/W. By taking localized THz fields into account, they also developed a quasi-static self-mixing model that describes the detector characteristics such as magnitude and polarity of the photocurrent.[133] In 2016, researchers from Massachusetts Institute of Technology and Agency for Science, Technology, and Research in Singapore proposed a new model for GaN HEMTs. This model can explain both polarity and magnitude of the photocurrent. This model helped to design of GaN-based HEMTs with asymmetric pads. Thanks to this model, the detection responsivity is enhanced by one order of magnitude.[134] The schematics of the cross section of the proposed GaN HEMT detector, antenna structures with traditional symmetric gate, and the proposed asymmetric gate are shown in Fig. 14.

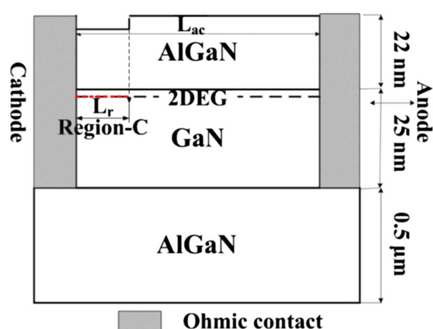

Fig. 13 The schematic structure of GaN-HEMT liked planar Gunn. Reprinted from Ref. 131, with permission of John Wiley and Sons publication.

2.10 *Antenna-Coupled Field-Effect Transistors for the Plasmonic Detection of THz Radiation*

In 2016, antenna-coupled field-effect transistors (TeraFETs) for the plasmonic detection of THz radiation were proposed and realized using a 0.25-μm AlGaN/GaN process.[135,136] The fabricated TeraFETs could detect frequencies up to 0.59 THz. This frequency is nearly twice of that of the implemented SiGe:C-based CMOS THz transmitters in 2015 that could emit frequencies up to 0.32 THz.[137,138] TeraFETs have the potential of being realized by CMOS technology and thus provide a promising building block for implementation of compact economical THz cameras. It is observed that such devices show good potential for edge detection and enhanced spatial resolution for THz imaging applications. Similar to asymmetrical GaN-based HEMTs proposed by Wang et al.[131], introduced in Sec. 2.9, Fig. 13, the TeraFETs are asymmetrical. This asymmetry is adopted due to the fact that it has been proven that asymmetric coupling is required for optimal power detection. The detector designs of bow-tie-antenna-coupled TeraFETs and the schematic of the TeraFET are shown in Fig. 15.

3 Characteristics and Physics of GAN in THz Regime

As the demand for using GaN-based devices for THz photonics is rising, the need for developing accurate techniques for characterization of this semiconductor material in THz frequency regime is emerging. In this section, a review on

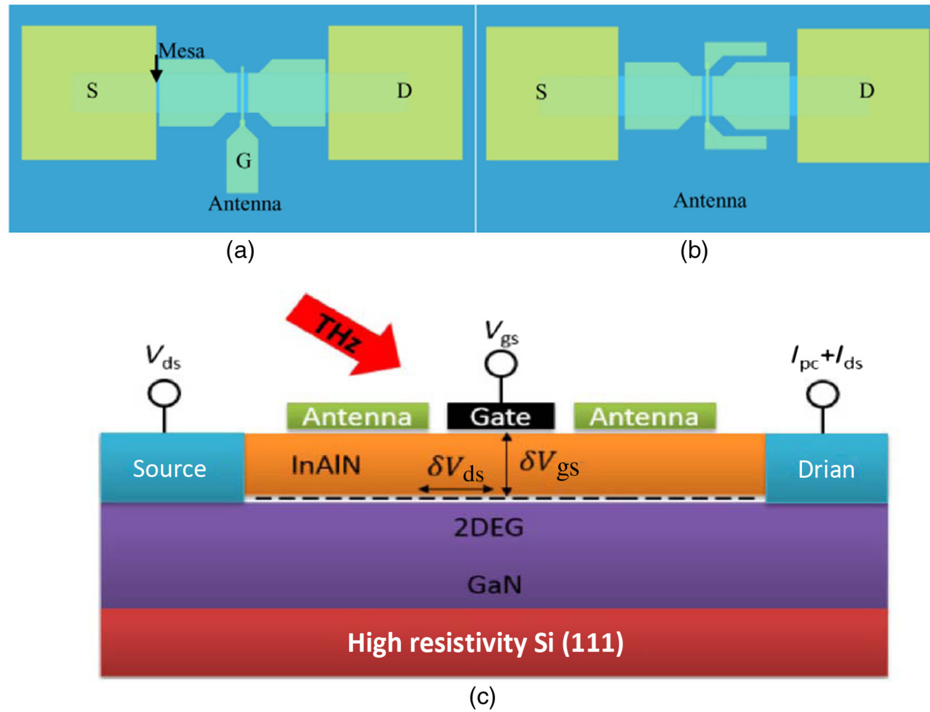

Fig. 14 Schematics of the antenna structures with (a) traditional symmetric gate and (b) proposed asymmetric gate. (c) The schematic of cross section of the proposed GaN HEMT detector. Reprinted from Ref. 134, with permission of Elsevier Ltd. publication.

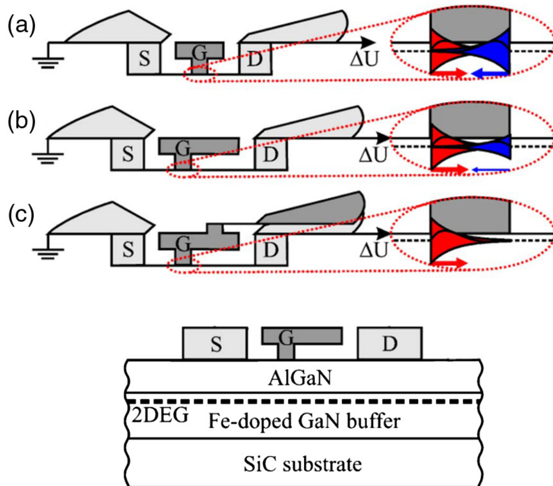

Fig. 15 Three detector designs (a)–(c) of bow-tie-antenna-coupled TeraFETs. The graph at the bottom displays a cross section of the respective AlGaN/GaN device. (a)–(c) Enlarged views of the gate regions illustrate the charge density waves propagating from the source side (red) and drain side (blue) of the gate for homogeneous illumination. Arrows indicate magnitude and direction of rectification responses of both waves. Reprinted from Ref. 136, with permission of IEEE.

the characterization of GaN in THz frequency range is provided.

3.1 *THz-Time-Domain Spectroscopy for Characterization of GaN*

The earliest comprehensive THz-TDS analysis of semiconductor materials has been reported by researchers from IBM in 1989.[139–141] However, the earliest THz-TDS characterization of the optical properties of GaN epitaxial films has been reported by Bu et al.[142] They observed the far-infrared transmission of the GaN/Al_2O_3 samples, and as a result, they could measure absorption coefficient, mobility, and carrier density in the 1- to 3-THz regime. In one of the early characterizations of GaN in THz frequency regime, which is reported by Zhang et al., the complex conductivity and dielectric function of GaN in the frequency range of 0.1 to 4 THz are reported.[143] Nagashima et al.[144,145] have reported a comprehensive electrical characterization of GaN thin films using THz TDS. In their work, DC resistivity of the GaN films with various free carrier densities and mobilities of the free carriers in lightly doped GaN films were calculated according to the to the Drude model. It is found that the temperature dependence of the mobilities for the lightly doped films shows a peak at 150 K, and the measured DC resistivity shows good agreement with those obtained by the conventional contact measurements. Tsai et al. reported indexes of refraction, extinction constants, and complex conductivities of the GaN film for frequencies ranging from 0.2 to 2.5 THz using THz-TDS. They used the Kohlrausch model fit which not only provides the mobility of the free carriers in the GaN film but also estimates the relaxation time distribution function and average relaxation time.[146] In the most recent work, the oscillating dielectric function at various temperatures within THz frequencies is obtained by Fang et al. in 2015. The concentration, electron lifetime, and temperature dependences of the point defects in GaN thin films were obtained. They reported that the concentration of the point defects decreases with the rise of temperature while the electron lifetime shows positive temperature dependence.[147]

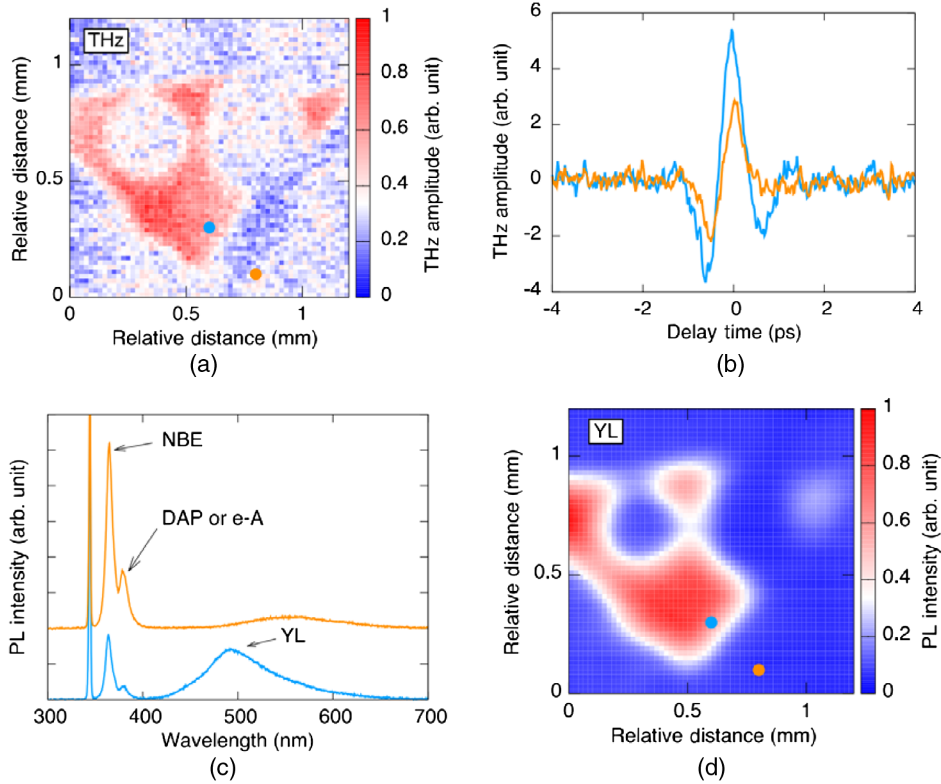

Fig. 16 (a) The LTEM image of *n*-type GaN with an excitation wavelength of 260 nm. (b) The THz waveforms at two points in (a). Line colors correspond to point colors in (a). (c) The PL spectra of GaN at two characteristic points shown in (d) as blue and orange points. The excitation wavelength is 345 nm. (d) PL 2-D mapping using the intensity of YL peak with the excitation wavelength of 345 nm.[152]

3.2 *Laser-Induced THz Emission Spectroscopy for Visualization of GaN Defect Density and Surface Potential*

Laser-induced THz emission spectroscopy (LTEM) has been used as an alternative to THz-TDS for characterization of optical and electrical properties of semiconductor materials.[148] LTEM has been also used for inspection of semiconductor devices.[149–151] Sakai et al.[152] have demonstrated laser-induced THz emission from the surface of GaN, which can be used for determination of the defect density and surface potential. They observed that when the GaN surface is excited by ultraviolet femtosecond laser pulses, the THz emission is enhanced by defects related to yellow luminescence (YL). As shown in Fig. 16, this phenomenon is explained by band bending as a result of trapped electrons at defect sites. The result of this visualization and its consistency with YL is shown in Fig. 16. The importance of this characterization technique is due to its applications for evaluation of the distribution of the nonradiative defects, which are undetectable with photoluminescence. Avoiding these defects leads to the realization of normally off GaN devices, which have an important part in energy-efficient power devices.

3.3 *THz Electro-Modulation Spectroscopy of GaN Electron Transport*

Engelbrecht et al.[153] have reported THz electromodulation spectroscopy for studying charge transport in *n*-type GaN. TDS significantly reduces mobility, and thus THz electromodulation spectroscopy is proposed as a promising tool for characterization of low doping densities where classical techniques are not efficient. As a result, the accessible frequency range extends from about 0.2 to 2.8 THz.

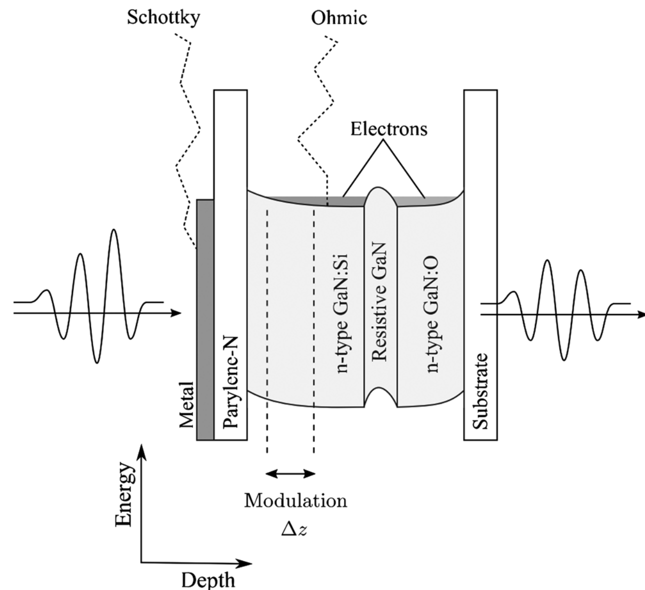

Fig. 17 Schematic band diagram of the devices in equilibrium. The sheet density of the electrons is modulated by the bias applied to the Schottky contact. The modulation affects absorption and dispersion of the THz pulses transmitted through the device. Reprinted from Ref. 153, with permission of AIP.

The experiment setup, which is shown in Fig. 17 includes GaN grown on sapphire by MOVPE. Schottky devices were fabricated for satisfying the requirement for switching of the electron sheet density $n_{2\text{-D}}$ within the semiconductor. This switching of $n_{2\text{-D}}$ is required for realizing THz electromodulation spectroscopy. In the mentioned work, the conductivity effective mass of the electrons and the relaxation times have been computed.

In addition to the mentioned properties, wide bandgap semiconductor materials and particularly GaN exhibit very interesting properties that can be utilized for implementing novel applications. In this respect, the unexpected effect of massive charge neutralization by enhanced exciton formation at very high plasma densities in wide-gap materials such as GaN has been demonstrated.[154] In another report, ultrafast internal field dynamics with lattice dynamics in GaN-based QWs are correlated and the measured THz strain amplitudes have been among the largest observed ultrafast photoacoustic generation.[155]

4 Conclusion

In this paper, the impact of the utilization of GaN for satisfying the industrial demands for compact, economical, high-resolution and high-power THz imaging and spectroscopy systems has been studied. It has been deduced that GaN-based devices can be utilized as the building blocks of the future THz systems that can provide THz radiation in the upper THz frequency band and with higher photon intensities. As a result, THz spectroscopy and imaging systems with higher depths of penetrations and resolutions can be realized. In this paper, a comprehensive survey on different GaN-based devices for generation and detection of THz radiation has been provided. This survey includes a review on plasma HFETs, NDRs, HDSDs, IMPATTs, QCLs, HEMTs, Gunn diodes, and TeraFETs. It has been highlighted that, due to the fact that the THz spectroscopy has not been widely available unless until a few decades ago, techniques for characterization of materials in THz frequency range still need to be developed. In this respect, a review of characterization techniques of GaN in THz frequency range has been provided in this paper as well. Particularly, THz-TDS, laser-induced THz emission spectroscopy, and THz-electromodulation spectroscopy for characterization of GaN are reviewed.

Acknowledgments

The shorter version of this paper was prepared as an invited conference paper for "Wide Bandgap Power Devices and Applications" section of "SPIE Optical Engineering and Applications," assigned to the author by Dr. Mehdi Anwar and Dr. Achyut Dutta.

The author welcomes research groups to provide him with their research outcomes in order to publish periodically updated reviews on the topic.

The author would like to thank the following prestigious researchers for providing him with their guidance and recent publications on the topic: Dr. Michael Shur, Dr. Tsong-Ru Tsai, Dr. Antanas Reklaitis, Dr. Roland Kersting, Dr. Chua Soo-Jin, Dr. Hideki Hirayama, Dr. Theodore D. Moustakas, Dr. Lin-An Yang, Dr. Roberto Paiella, Dr. Hua Qin, and Dr. Viktor Krozer.

References

1. J. I. Pankove, E. A. Miller, and J. E. Berkeyheiser, "GaN electroluminescent diodes," in *Int. Electron Devices Meeting*, Vol. 17, pp. 78–78 (1971).
2. T. Yanagisawa, "Changes in properties of GaN blue light-emitting diodes over time," *Electron. Lett.* **22**, 846–847 (1986).
3. G. Venkataramanan and D. M. Divan, "Pulse width modulation with resonant DC link converters," in *Conf. Record of the IEEE Industry Applications Society Annual Meeting*, pp. 984–990, IEEE (1990).
4. M. Fathipour et al., "A novel double field-plate power high electron mobility transistor based on AlGaN/GaN for performance improvement," in *Int. Conf. on Signal Processing, Communication, Computing and Networking Technologies*, pp. 272–276 (2011).
5. K. Ahi, "Developing next generation of electric grids for fulfilling deficiencies of conventional grids in supporting today's requirements," in *Int. Conf. on Power Engineering, Energy and Electrical Drives*, pp. 1–7, IEEE (2011).
6. H. Nasiri et al., "Dynamic modeling and simulation of transmotor based series-parallel HEV applied to Toyota Prius 2004," in *10th Int. Conf. on Environment and Electrical Engineering*, pp. 1–4, IEEE (2011).
7. K. Ahi, "Control and design of a modular converter system for vehicle applications," Leibniz Universität Hannover (2012).
8. B. B. Hu and M. C. Nuss, "Imaging with terahertz waves," *Opt. Lett.* **20**, 1716–1718 (1995).
9. J. L. Prince and J. Links, *Medical Imaging Signals and Systems*, Pearson Prentice Hall, Upper Saddle River (2006).
10. X. Wan et al., "SEB hardened power MOSFETs with high-K dielectrics," *IEEE Trans. Nucl. Sci.* **62**, 2830–2836 (2015).
11. C. L. K. Dandolo and P. U. Jepsen, "Wall painting investigation by means of non-invasive terahertz time-domain imaging (THz-TDI): inspection of subsurface structures buried in historical plasters," *J. Infrared Millimeter Terahertz Waves* **37**, 198–208 (2016).
12. L. V. Titova et al., "Intense THz pulses cause H2AX phosphorylation and activate DNA damage response in human skin tissue," *Biomed. Opt. Express* **4**, 559–568 (2013).
13. E. V. Demidova et al., "Impact of terahertz radiation on stress-sensitive genes of E. coli cell," *IEEE Trans. Terahertz Sci. Technol.* **6**, 435–441 (2016).
14. L. V. Titova et al., "Intense THz pulses down-regulate genes associated with skin cancer and psoriasis: a new therapeutic avenue?" *Sci. Rep.* **3**, 1–6 (2013).
15. K. Ahi et al., "Terahertz characterization of electronic components and comparison of terahertz imaging with x-ray imaging techniques," *Proc. SPIE* **9483**, 94830K (2015).
16. D. M. Mittleman et al., "T-ray tomography," *Opt. Lett.* **22**, 904–906 (1997).
17. K. Ahi, S. Shahbazmohamadi, and N. Asadizanjani, "Quality control and authentication of packaged integrated circuits using enhanced-spatial-resolution terahertz time-domain spectroscopy and imaging," *Opt. Lasers Eng.* (2017).
18. Z. Ali and B. Florent, "Potential of chipless authentication based on randomness inherent in fabrication process for RF and THz," in *11th European Conf. on Antennas and Propagation (EUCAP)* (2017).
19. K. Ahi and M. Anwar, "A novel approach for enhancement of the resolution of terahertz measurements for quality control and counterfeit detection," in *Diminishing Manufacturing Sources and Material Shortages (DMSMS)*, Phoenix, Arizona (2015).
20. H. Zhang et al., "Numerical and experimental analyses for natural and non-natural impacted composites via thermographic inspection, ultrasonic C-scan and terahertz imaging," *Proc. SPIE* **10214**, 102140I (2017).
21. I. S. Gregory et al., "Continuous-wave terahertz system with a 60 dB dynamic range," *Appl. Phys. Lett.* **86**, 204104 (2005).
22. N. S. Balbekin et al., "Nondestructive monitoring of aircraft composites using terahertz radiation," *Proc. SPIE* **9448**, 94482D (2015).
23. T. Hagelschuer et al., "High-spectral-resolution terahertz imaging with a quantum-cascade laser," *Opt. Express* **24**, 13839–13849 (2016).
24. E. V. Yakovlev et al., "Non-destructive evaluation of polymer composite materials at the manufacturing stage using terahertz pulsed spectroscopy," *IEEE Trans. Terahertz Sci. Technol.* **5**, 810–816 (2015).
25. U. Schmidhammer and P. Jeunesse, "Pulsed THz imaging for non-destructive testing of adhesive bonds," in *39th Int. Conf. on Infrared, Millimeter, and Terahertz Waves (IRMMW-THz)*, pp. 1–2, IEEE (2014).
26. X. Neiers, P. Jeunesse, and U. Schmidhammer, "Rapid control of machined glass fiber reinforced plastics by single shot terahertz time domain spectroscopy," in *40th Int. Conf. on Infrared, Millimeter, and Terahertz Waves (IRMMW-THz)*, pp. 1–2, IEEE (2015).
27. K. Ahi and M. Anwar, "Modeling of terahertz images based on x-ray images: a novel approach for verification of terahertz images and identification of objects with fine details beyond terahertz resolution," *Proc. SPIE* **9856**, 985610 (2016).
28. P. Lopato and T. Chady, "Terahertz detection and identification of defects in layered polymer composites and composite coatings," *Nondestruct. Test. Eval.* **28**, 28–43 (2013).
29. C. Seco-Martorell et al., "Goya's artwork imaging with terahertz waves," *Opt. Express* **21**, 17800–17805 (2013).

30. V. P. Wallace et al., "Three-dimensional imaging of optically opaque materials using nonionizing terahertz radiation," *J. Opt. Soc. Am. A* **25**, 3120–3133 (2008).
31. J. B. Perraud et al., "Terahertz imaging and tomography as efficient instruments for testing polymer additive manufacturing objects," *Appl. Opt.* **55**, 3462–3467 (2016).
32. H. Balacey et al., "Advanced processing sequence for 3-D THz imaging," *IEEE Trans. Terahertz Sci. Technol.* **6**, 191–198 (2016).
33. C. Dietlein, Z. Popovic, and E. N. Grossman, "Aqueous blackbody calibration source for millimeter-wave/terahertz metrology," *Appl. Opt.* **47**, 5604–5615 (2008).
34. P. Lopato, "Double-sided terahertz imaging of multilayered glass fiber-reinforced polymer," *Appl. Sci.* **7**, 661 (2017).
35. F. Rutz et al., "Terahertz quality control of polymeric products," *Int. J. Infrared Millimeter Waves* **27**, 547–556 (2006).
36. K. Ahi and M. Anwar, "Advanced terahertz techniques for quality control and counterfeit detection," *Proc. SPIE* **9856**, 98560G (2016).
37. Z. Popović and E. N. Grossman, "THz metrology and instrumentation," *IEEE Trans. Terahertz Sci. Technol.* **1**, 133–144 (2011).
38. E. N. Grossman, A. Luukanen, and A. J. Miller, "Terahertz active direct detection imagers," *Proc. SPIE* **5411**, 68–77 (2004).
39. E. N. Grossman, "Active millimeter-wave imaging for concealed weapons detection," *Proc. SPIE* **5077**, 62–70 (2003).
40. E. Grossman et al., "Passive terahertz camera for standoff security screening," *Appl. Opt.* **49**, E106–E120 (2010).
41. V. A. Trofimov et al., "New algorithm for detection of dangerous objects hidden on a human body using passive THz camera," *Proc. SPIE* **9993**, 999305 (2016).
42. V. A. Trofimov et al., "Concealed object detection using the passive THz image without its viewing," *Proc. SPIE* **9830**, 98300E (2016).
43. I. N. Dolganova et al., "A hybrid continuous-wave terahertz imaging system," *Rev. Sci. Instrum.* **86**, 113704 (2015).
44. M. Kowalski and M. Kastek, "Comparative studies of passive imaging in terahertz and mid-wavelength infrared ranges for object detection," *IEEE Trans. Inf. Forensics Secur.* **11**, 2028–2035 (2016).
45. M. Kowalski et al., "Passive imaging of concealed objects in terahertz and long-wavelength infrared," *Appl. Opt.* **54**, 3826–3833 (2015).
46. J.-P. Guillet et al., "Art painting diagnostic before restoration with terahertz and millimeter waves," *J. Infrared Millimeter Terahertz Waves* **38**, 369–379 (2017).
47. H. Zhang et al., "Non-destructive investigation of paintings on canvas by continuous wave terahertz imaging and flash thermography," *J. Nondestr. Eval.* **36**, 34 (2017).
48. J. P. Guillet et al., "Low-frequency noise effect on terahertz tomography using thermal detectors," *Appl. Opt.* **54**, 6758–6762 (2015).
49. B. Ferguson et al., "T-ray computed tomography," *Opt. Lett.* **27**, 1312 (2002).
50. N. Rothbart et al., "Fast 2-D and 3-D terahertz imaging with a quantum-cascade laser and a scanning mirror," *IEEE Trans. Terahertz Sci. Technol.* **3**, 617–624 (2013).
51. J. B. Perraud et al., "Terahertz imaging and tomography as efficient instruments for testing polymer additive manufacturing objects," *Appl. Opt.* **55**, 3462–3467 (2016).
52. M. W. Ayech and D. Ziou, "Terahertz image segmentation using k-means clustering based on weighted feature learning and random pixel sampling," *Neurocomputing* **175**, 243–264 (2016).
53. E. A. Strepitov et al., "Analysis of spectral characteristics of normal fibroblasts and fibroblasts cultured with cancer cells in terahertz frequency range," in *Progress in Electromagnetics Research Symp. Proc.*, pp. 1707–1710 (2014).
54. M. V. Duka et al., "Numerical and experimental studies of mechanisms underlying the effect of pulsed broadband terahertz radiation on nerve cells," *Quantum Electron.* **44**, 707–712 (2014).
55. K. I. Zaytsev et al., "In vivo terahertz spectroscopy of pigmentary skin nevi: pilot study of non-invasive early diagnosis of dysplasia," *Appl. Phys. Lett.* **106**, 053702 (2015).
56. K. I. Zaytsev et al., "Highly accurate in vivo terahertz spectroscopy of healthy skin: variation of refractive index and absorption coefficient along the human body," *IEEE Trans. Terahertz Sci. Technol.* **5**, 817–827 (2015).
57. K. I. Zaytsev et al., "Invariant embedding technique for medium permittivity profile reconstruction using terahertz time-domain spectroscopy," *Opt. Eng.* **52**, 068203 (2013).
58. Z. J. Thompson et al., "Terahertz-triggered phase transition and hysteresis narrowing in a nanoantenna patterned vanadium dioxide film," *Nano Lett.* **15**, 5893–5898 (2015).
59. B. Lee et al., "Anisotropic high-field terahertz response of free-standing carbon nanotubes," *Appl. Phys. Lett.* **108**, 241111 (2016).
60. M. J. Paul et al., "Terahertz induced transparency in single-layer graphene," *Appl. Phys. Lett.* **105**, 221107 (2014).
61. P. Lopato, "Estimation of layered materials dielectric parameters using pulsed terahertz technique," *Int. J. Appl. Electromagn. Mech.* **43**, 161–168 (2013).
62. K. Kawase et al., "Non-destructive terahertz imaging of illicit drugs using spectral fingerprints," *Opt. Express* **11**, 2549–2554 (2003).
63. J. Dong, A. Locquet, and D. S. Citrin, "Depth resolution enhancement of terahertz deconvolution by autoregressive spectral extrapolation," *Opt. Lett.* **42**, 1828–1831 (2017).
64. K. Su, Y.-C. Shen, and J. A. Zeitler, "Terahertz sensor for non-contact thickness and quality measurement of automobile paints of varying complexity," *IEEE Trans. Terahertz Sci. Technol.* **4**, 432–439 (2014).
65. N. V. Petrov et al., "Application of terahertz pulse time-domain holography for phase imaging," *IEEE Trans. Terahertz Sci. Technol.* **6**, 464–472 (2016).
66. M. S. Heimbeck et al., "Terahertz digital holographic imaging of voids within visibly opaque dielectrics," *IEEE Trans. Terahertz Sci. Technol.* **5**, 110–116 (2015).
67. Y. Zhang et al., "Terahertz digital holography," *Strain* **44**, 380–385 (2008).
68. N. S. Balbekin et al., "The modeling peculiarities of diffractive propagation of the broadband terahertz two-dimensional field," *Phys. Proc.* **73**, 49–53 (2015).
69. B. E. A. Saleh and M. C. Teich, *Fundamentals of Photonics*, 2nd ed., p. 1200, Wiley, New York (2007).
70. K. Ahi and M. Anwar, "A survey on GaN-based devices for terahertz photonics," *Proc. SPIE* **9957**, 99570A (2016).
71. R. I. Stantchev et al., "Noninvasive, near-field terahertz imaging of hidden objects using a single-pixel detector," *Sci. Adv.* **2**, e1600190 (2016).
72. V. A. Trofimov and V. V. Trofimov, "New way for concealed object detection using passive THz images without their viewing," *Proc. SPIE* **9651**, 96510A (2015).
73. V. A. Trofimov et al., "Increasing the instrumental resolution of a commercially available passive THz camera due to computer treatment of image," in *Proc. of 5th Global Symp. on Millimeter-Waves*, pp. 427–430, IEEE (2012).
74. M. S. Kulya et al., "Computational terahertz imaging with dispersive objects," *J. Mod. Opt.* **64**, 1283–1288 (2017).
75. A. Siemion et al., "Off-axis metallic diffractive lens for terahertz beams," *Opt. Lett.* **36**, 1960–1962 (2011).
76. A. Siemion et al., "Diffractive paper lens for terahertz optics," *Opt. Lett.* **37**, 4320–4322 (2012).
77. A. Siemion et al., "THz beam shaping based on paper diffractive optics," *IEEE Trans. Terahertz Sci. Technol.* **6**, 568–575 (2016).
78. A. I. Hernandez-Serrano et al., "Fabrication of gradient-refractive-index lenses for terahertz applications by three-dimensional printing," *J. Opt. Soc. Am. B* **33**, 928–931 (2016).
79. K. Ahi and M. Anwar, "Developing terahertz imaging equation and enhancement of the resolution of terahertz images using deconvolution," *Proc. SPIE* **9856**, 98560N (2016).
80. K. Ahi, "Mathematical modeling of THz point spread function and simulation of THz imaging systems," *IEEE Trans. Terahertz Sci. Technol.* (2017).
81. N. V. Chernomyrdin et al., "Solid immersion terahertz imaging with sub-wavelength resolution," *Appl. Phys. Lett.* **110**, 221109 (2017).
82. N. V. Chernomyrdin et al., "Wide-aperture aspherical lens for high-resolution terahertz imaging," *Rev. Sci. Instrum.* **88**, 014703 (2017).
83. A. Kannegulla et al., "Photo-induced spatial modulation of THz waves: opportunities and limitations," *Opt. Express* **23**, 32098–32112 (2015).
84. A. Kannegulla et al., "Coded-aperture imaging using photo-induced reconfigurable aperture arrays for mapping terahertz beams," *IEEE Trans. Terahertz Sci. Technol.* **4**, 321–327 (2014).
85. A. Kannegulla and L.-J. Cheng, "Subwavelength focusing of terahertz waves in silicon hyperbolic metamaterials," *Opt. Lett.* **41**, 3539–3542 (2016).
86. W. Terashima and H. Hirayama, "GaN-based terahertz quantum cascade lasers," *Proc. SPIE* **9483**, 948304 (2015).
87. B. Mirzaei, A. Rostami, and H. Baghban, "Terahertz dual-wavelength quantum cascade laser based on GaN active region," *Opt. Laser Technol.* **44**, 378–383 (2012).
88. M. Marso, "GaN for THz sources," in *Eighth Int. Conf. on Advanced Semiconductor Devices and Microsystems*, pp. 147–154 (2010).
89. D. Pavlidis, "GaN THz electronics," in *European Gallium Arsenide and Related III–V Compounds Application Symp.*, pp. 551–554 (2004).
90. J. Li et al., "Efficient terahertz wave generation from GaP crystals pumped by chirp-controlled pulses from femtosecond photonic crystal fiber amplifier," *Appl. Phys. Lett.* **104**, 031117 (2014).
91. J. Li et al., "Generation of 0.3 mW high-power broadband terahertz pulses from GaP crystal pumped by negatively chirped femtosecond laser pulses," *Laser Phys. Lett.* **10**, 125404 (2013).
92. M. Tonouchi, "Cutting-edge terahertz technology," *Nat. Photonics* **1**, 97–105 (2007).
93. T. Otsuji and M. Shur, "Terahertz plasmonics: good results and great expectations," *IEEE Microwave Mag.* **15**, 43–50 (2014).
94. H. Hirayama et al., "Recent progress and future prospects of THz quantum-cascade lasers," *Proc. SPIE* **9382**, 938217 (2015).
95. M. Shur, "AlGaN/GaN plasmonic terahertz electronic devices," *J. Phys.* **486**, 012025 (2014).

96. M. I. Dyakonov and M. S. Shur, "Plasma wave electronics: novel terahertz devices using two dimensional electron fluid," *IEEE Trans. Electron. Devices* **43**, 1640–1645 (1996).
97. L. O. Hocker, "Absolute frequency measurement and spectroscopy of gas laser transitions in the far infrared," *Appl. Phys. Lett.* **10**, 147–149 (1967).
98. M. Duguay and J. Hansen, "Optical frequency shifting of a mode-locked laser beam," in *Int. Electron Devices Meeting*, Vol. 13, p. 34 (1967).
99. J.-Q. Lu et al., "Detection of microwave radiation by electronic fluid in AlGaN/GaN heterostructure field effect transistors," in *Proc. IEEE/Cornell Conf. on Advanced Concepts in High Speed Semiconductor Devices and Circuits*, pp. 211–217, IEEE (1997).
100. W. Knap et al., "Nonresonant detection of terahertz radiation in field effect transistors," *J. Appl. Phys.* **91**, 9346–9353 (2002).
101. M. Dyakonov and M. Shur, "Detection, mixing, and frequency multiplication of terahertz radiation by two-dimensional electronic fluid," *IEEE Trans. Electron. Devices* **43**, 380–387 (1996).
102. M. S. Shur and J.-Q. Lu, "Terahertz sources and detectors using two-dimensional electronic fluid in high electron-mobility transistors," *IEEE Trans. Microwave Theory Tech.* **48**, 750–756 (2000).
103. S. J. Allen, D. C. Tsui, and R. A. Logan, "Observation of the two-dimensional plasmon in silicon inversion layers," *Phys. Rev. Lett.* **38**, 980 (1977).
104. D. C. Tsui, E. Gornik, and R. A. Logan, "Far infrared emission from plasma oscillations of Si inversion layers," *Solid State Commun.* **35**, 875–877 (1980).
105. A. El Fatimy et al., "Terahertz detection by GaN/AlGaN transistors," *Electron. Lett.* **42**, 1342 (2006).
106. J. Faist et al., "Quantum cascade laser," *Science* **264**, 553–556 (1994).
107. R. Köhler et al., "Terahertz semiconductor-heterostructure laser," *Nature* **417**, 156–159 (2002).
108. B. S. Williams et al., "Operation of terahertz quantum-cascade lasers at 164 K in pulsed mode and at 117 K in continuous-wave mode," *Opt. Express* **13**, 3331–3339 (2005).
109. E. Bellotti et al., "Monte Carlo simulation of terahertz quantum cascade laser structures based on wide-bandgap semiconductors," *J. Appl. Phys.* **105**, 113103 (2009).
110. E. Bellotti et al., "Monte Carlo study of GaN versus GaAs terahertz quantum cascade structures," *Appl. Phys. Lett.* **92**, 101112 (2008).
111. F. Sudradjat et al., "Sequential tunneling transport characteristics of GaN/AlGaN coupled-quantum-well structures," *J. Appl. Phys.* **108**, 103704 (2010).
112. D. Turchinovich et al., "Ultrafast polarization dynamics in biased quantum wells under strong femtosecond optical excitation," *Phys. Rev. B* **68**, 241307 (2003).
113. D. Turchinovich, B. S. Monozon, and P. U. Jepsen, "Role of dynamical screening in excitation kinetics of biased quantum wells: nonlinear absorption and ultrabroadband terahertz emission," *J. Appl. Phys.* **99**, 013510 (2006).
114. H. Hirayama et al., "Recent progress and future prospects of THz quantum-cascade lasers," *Proc. SPIE* **9382**, 938217 (2015).
115. W. Terashima and H. Hirayama, "Terahertz frequency emission with novel quantum cascade laser designs," *Proc. SPIE* 11–13 (2015).
116. S. Miho, T.-T. Lin, and H. Hirayama, "1.9 THz selective injection design quantum cascade laser operating at extreme higher temperature above the k_BT line," *Phys. Status Solidi C* **10**, 1448–1451 (2013).
117. T.-T. Lin and H. Hirayama, "Improvement of operation temperature in GaAs/AlGaAs THz-QCLs by utilizing high Al composition barrier," *Phys. Status Solidi C* **10**, 1430–1433 (2013).
118. T.-T. Lin, L. Ying, and H. Hirayama, "Threshold current density reduction by utilizing high-al-composition barriers in 3.7 THz GaAs/$Al_xGa_{1-x}As$ quantum cascade lasers," *Appl. Phys. Express* **5**, 012101 (2012).
119. C. Edmunds et al., "Terahertz intersubband absorption in non-polar m-plane AlGaN/GaN quantum wells," *Appl. Phys. Lett.* **105**, 021109 (2014).
120. M. Beeler, E. Trichas, and E. Monroy, "III-nitride semiconductors for intersubband optoelectronics: a review," *Semicond. Sci. Technol.* **28**, 074022 (2013).
121. M. Beeler et al., "Pseudo-square AlGaN/GaN quantum wells for terahertz absorption," *Appl. Phys. Lett.* **105**, 131106 (2014).
122. H. Durmaz et al., "Terahertz intersubband photodetectors based on semi-polar GaN/AlGaN heterostructures," *Appl. Phys. Lett.* **108**, 201102 (2016).
123. S. Krishnamurthy et al., "Bandstructure effect on high-field transport in GaN and GaAlN," *Appl. Phys. Lett.* **71**, 1999–2001 (1997).
124. B. E. Foutz et al., "Comparison of high field electron transport in GaN and GaAs," *Appl. Phys. Lett.* **70**, 2849–2851 (1997).
125. E. Alekseev and D. Pavlidis, "GaN Gunn diodes for THz signal generation," in *IEEE MTT-S Int. Microwave Symp. Digest (Cat. No. 00CH37017)*, Vol. 3, pp. 1905–1908 (2000).
126. E. Alekseev et al., "GaN-based NDR devices for THz generation," in *Proc. of the Eleventh Int. Symp. on Space Terahertz Technology*, p. 162 (2000).
127. D. Veksler et al., "GaN heterodimensional Schottky diode for THz detection," in *5th IEEE Conf. Sensors*, pp. 323–326, IEEE (2006).
128. W. C. B. Peatman, T. W. Crowe, and M. Shur, "A novel Schottky/2-DEG diode for millimeter- and submillimeter-wave multiplier applications," *IEEE Electron. Device Lett.* **13**, 11–13 (1992).
129. A. Reklaitis, "Monte Carlo study of hot-carrier transport in bulk wurtzite GaN and modeling of a near-terahertz impact avalanche transit time diode," *J. Appl. Phys.* **95**, 7925–7935 (2004).
130. A. Reklaitis and L. Reggiani, "Giant suppression of avalanche noise in GaN double-drift impact diodes," *Solid State Electron.* **49**, 405–408 (2005).
131. Y. Wang et al., "Modulation of the domain mode in GaN-based planar Gunn diode for terahertz applications," *Phys. Status Solidi C* **13**, 382–385 (2016).
132. J. D. Sun et al., "High-responsivity, low-noise, room-temperature, self-mixing terahertz detector realized using floating antennas on a GaN-based field-effect transistor," *Appl. Phys. Lett.* **100**, 013506 (2012).
133. R. A. Lewis et al., "Probing and modelling the localized self-mixing in a GaN/AlGaN field-effect terahertz detector," *Appl. Phys. Lett.* **100**, 173513 (2012).
134. H. Hou et al., "Modelling of GaN HEMTs as terahertz detectors based on self-mixing," *Proc. Eng.* **141**, 98–102 (2016).
135. M. Bauer et al., "High-sensitivity wideband THz detectors based on GaN HEMTs with integrated bow-tie antennas," in *10th European Microwave Integrated Circuits Conf. (EuMIC)*, pp. 1–4, IEEE (2015).
136. S. Boppel et al., "0.25-μm GaN TeraFETs optimized as THz power detectors and intensity-gradient sensors," *IEEE Trans. Terahertz Sci. Technol.* **6**, 348–350 (2016).
137. R. Han et al., "25.5 A 320 GHz phase-locked transmitter with 3.3 mW radiated power and 22.5 dBm EIRP for heterodyne THz imaging systems," in *IEEE Int. Solid-State Circuits Conf.–(ISSCC) Digest of Technical Papers*, Vol. 50, pp. 1–3, IEEE (2015).
138. R. Han et al., "A SiGe terahertz heterodyne imaging transmitter with 3.3 mW radiated power and fully-integrated phase-locked loop," *IEEE J. Solid State Circuits* **50**, 2935–2947 (2015).
139. M. Van Exter and D. Grischkowsky, "Carrier dynamics of electrons and holes in moderately doped silicon," *Phys. Rev. B* **41**, 12140–12149 (1990).
140. D. Grischkowsky et al., "Far-infrared time-domain spectroscopy with terahertz beams of dielectrics and semiconductors," *J. Opt. Soc. Am. B* **7**, 2006–2015 (1990).
141. N. Katzenellenbogen and D. Grischkowsky, "Electrical characterization to 4 THz of N- and P-type GaAs using THz time-domain spectroscopy," *Appl. Phys. Lett.* **61**, 840–842 (1992).
142. Y. Bu et al., "Optical properties of GaN epitaxial films grown by low-pressure chemical vapor epitaxy using a new nitrogen source: hydrazoic acid (HN_3)," *Appl. Phys. Lett.* **66**, 2433–2435 (1995).
143. A. K. Azad, W. Zhang, and D. Grischkowsky, "Terahertz carrier dynamics and dielectric response of n-type GaN," in *Conf. on Lasers and Electro-Optics (CLEO)*, p. 3 (2003).
144. T. Nagashima, K. Takata, and M. Hangyo, "Electrical characterization of GaN thin films using terahertz-time domain spectroscopy," in *Twenty Seventh Int. Conf. on Infrared and Millimeter Waves*, pp. 247–248, IEEE (2002).
145. T. Nagashima et al., "Measurement of electrical properties of GaN thin films using terahertz-time domain spectroscopy," *Jpn. J. Appl. Phys.* **44**, 926–931 (2005).
146. T.-R. Tsai et al., "Terahertz response of GaN thin films," *Opt. Express* **14**, 4898–4907 (2006).
147. H. Fang et al., "Temperature dependence of the point defect properties of GaN thin films studied by terahertz time-domain spectroscopy," *Sci. China Phys. Mech. Astron.* **56**, 2059–2064 (2013).
148. T. Kondo et al., "Terahertz radiation from (111) InAs surface using 1.55 μm femtosecond laser pulses," *Jpn. J. Appl. Phys.* **38**, L1035–L1037 (1999).
149. T. Kiwa et al., "Laser terahertz-emission microscope for inspecting electrical faults in integrated circuits," *Opt. Lett.* **28**, 2058–2060 (2003).
150. K. Nikawa et al., "Non-electrical-contact LSI failure analysis using non-bias laser terahertz emission microscope," in *18th IEEE Int. Symp. on the Physical and Failure Analysis of Integrated Circuits (IPFA)*, pp. 1–5 (2011).
151. N. Hidetoshi et al., "Imaging of a polycrystalline silicon solar cell using a laser terahertz emission microscope," *Appl. Phys. Express* **5**, 112301 (2012).
152. Y. Sakai et al., "Visualization of GaN surface potential using terahertz emission enhanced by local defects," *Sci. Rep.* **5**, 13860 (2015).
153. S. G. Engelbrecht et al., "Terahertz electromodulation spectroscopy of electron transport in GaN," *Appl. Phys. Lett.* **106**, 092107 (2015).
154. A. Hangleiter et al., "Efficient formation of excitons in a dense electron-hole plasma at room temperature," *Phys. Rev. B* **92**, 241305 (2015).

155. P. J. S. van Capel et al., "Correlated terahertz acoustic and electromagnetic emission in dynamically screened InGaN/GaN quantum wells," *Phys. Rev. B* **84**, 085317 (2011).

Kiarash Ahi received his MSc degree in electrical and information engineering from Leibniz University of Hannover, Germany, in 2012, and his PhD in electrical and computer engineering from the University of Connecticut, USA, in 2017. He is currently a senior design engineer at GlobalFoundries located at Hudson Valley Research Park (formerly IBM Microelectronics), East Fishkill, New York, USA. His research includes developing resolution enhancement techniques in collaboration with design rule, lithography, etch, and metrology teams to obtain the data needed for exposure source optimization and optical proximity correction.